Frontiers in Offshore Geotechnics III – Meyer (Ed.)
© 2015 Taylor & Francis Group, London, ISBN: 978-1-138-02848-7

Boulder-soil-pile dynamic interaction

A. Holeyman
Université Catholique de Louvain, Louvain-la-Neuve, Belgium

P. Peralta & N. Charue
Fugro GeoConsulting, Brussels, Belgium

ABSTRACT: A mechanical model is suggested herein to explore the interaction between a boulder and a pile being driven, taking into account the properties of the rock forming the boulder and the embedding geological formation. A one-dimensional model is considered as a first attempt, with a view to integrate it into a classical one-dimensional wave-equation representation of the pile being driven. A typical case of a tubular pile driven into stiff glacial till by a hydraulic hammer is investigated. The proposed model is shown to highlight the influence of pile dimensions, boulder size, and hammer energy on the potential damage to the pile toe. Conclusions can be drawn in terms of an optimal range of hammer operational setting, depending on expected boulder size.

1 INTRODUCTION

Damage to the pile tip may be encountered during the different pile driving installation stages. Pile tip buckling, ovality, deformation or denting could result from lifting and handling operations and driving into the subsoil. Whilst there are standard protocols to mitigate and check occurrence of damage to the pile during fabrication and handling, investigation of pile tip damage during driving and incremental penetration into the soil is not typically performed.

However, damage to the pile is a real risk that can occur when the pile hits a hard stratum or encounters objects such as boulders in the subsoil as it is being driven. Once an initial imperfection to the pile tip has been initiated, progressive pile failure may develop. Full pile failure with "severely crushed" tips and the resulting consequences have been reported for the Valhall Water Injection Platform jacket in the North Sea, Norwegian Sector (Alm et al. 2004) and for the Goodwyn A platform on the North West Shelf of Australia (Barbour & Erbrich 1995, Erbrich et al. 2010). This type of failure or pile damage propagation is likely to occur for thin-walled piles and very stiff subsoil conditions such as very dense sand, stiff boulder-clay formations, and stiff chalk strata (Barbour & Erbrich 1994, Aldridge et al. 2005). Hence, the potential for pile damage may be especially critical for very large diameter tubular piles such as monopiles with increasingly higher D/t or diameter to wall thickness ratios, which are used to support offshore wind turbines and driven into boulder prone formations such as stiff glacial till.

This paper focuses on a model based on the 1D wave theory to predict the likely initiation of pile tip damage as it encounters a boulder during pile driving in stiff boulder clay formations (till) and the ensuing risk of pile damage propagation. Several limit states are considered in the following sections focusing on the pile, the medium surrounding the boulder, and finally the boulder itself. The case for a large-diameter pile with $D = 6$ m is investigated.

2 PILE LIMIT STATES

2.1 *Modes of pile failure*

The term "damage" is normally associated with failure, yielding or buckling, but may generally encompass any pile imperfections such as denting or ovalisation, etc. The following seeks to clarify the pile failure modes and the more general pile imperfections.

Axial pile buckling implies yielding of the pile material due to an axial stress while ring or shell buckling is yielding due to radial pressures. If the pile fails or yields at the tip due to an axial force encountered, e.g. when it hits a hard stratum or object, this is known as pile tip local buckling. Pile imperfections include ovality (initial out-of-circularity) or dents. While imperfections of the pile do not necessarily imply material failure or buckling, these may lead to axial and shell buckling of the pile.

Another pile failure phenomenon is known as damage propagation or propagation buckling. Damage propagation is the progressive yielding of the pile during driving, stemming from an initial imperfection at the pile tip and developing into full pile failure. Full pile failure may be a combination of axial and shell buckling and is typically evident by crushed

pile ends with axial crimping and/or closed pile ends due to fully-formed shell buckling failure resulting in a peanut form cross-section, hence the synonymous term "peanut buckling".

2.2 *Existing assessment methods*

Limiting stresses from solutions of classical elastic equations for tubular systems may be used to assess pure axial or shell buckling of the pile. However, damage to the pile due to driving and penetration into the subsoil is a more complex failure mechanism that must account for the soil response.

An HSE (2001) study on pile tip integrity provides solutions based on classical mechanics for pure axial and shell buckling and the maximum pile tip force F_{tip} to cause a local dent:

$$F_{tip} = 1.2\sigma_y t^2 \quad (1)$$

with σ_y = pile yield stress and t = pile wall thickness.

Aldridge et al. (2005) investigated the lateral and near axial forces, $F_{lateral}$ and F_{axial}, at the pile tip to initiate a local dent by applying upper bound theory for an assumed plastic hinge mechanism and proposed similar expressions:

$$F_{lateral} = 1.4\sigma_y t^2 \quad (2)$$

$$F_{axial} = 2.8\sigma_y t^2 \quad (3)$$

Based on solutions for inward deflection of a ring, similar to ovalisation, the above authors also proposed expressions to compare the pile diameter to thickness ratio D/t with the pile and soil stiffness, E_p and E_s, and yield strengths σ_y and σ_{soil}, respectively, that would likely lead to pile damage propagation.

The pile and soil conditions that would lead to progressive pile damage were investigated in more detail by Barbour and Erbrich (1995) and Erbrich et al. (2010), who developed a numerical model BASIL with a user implemented soil "extrusion" algorithm to more accurately predict progressive damage. The numerical analysis tracks the growth of an initial imperfection of a pile and establishes whether this will lead to a structural collapse.

2.3 *Proposed 1-D wave equation model of pile-boulder interaction*

This study deals with the premise that encountering a boulder during driving as the pile penetrates into the subsoil will cause a contact force at the pile tip that may be large enough to initiate a local imperfection or even local pile tip buckling. The magnitude of the contact force depends on the hammer settings, properties of the pile, boulder, and embedding soil.

The boulder-pile interaction is a dynamic problem and is proposed to be modeled based on the 1D wave theory. Figure 1 illustrates the considered situation and

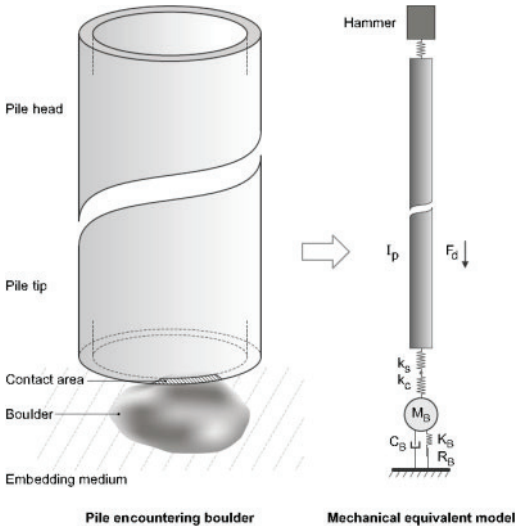

Figure 1. Pile-boulder-soil model.

the assumed mechanical model representation in 1D, where I_p is the pile impedance, $F_d\downarrow$ is the hammer generated incoming wave force, k_s and k_c are respectively the pile contact stiffness and boulder contact stiffness, M_B is the boulder mass, C_B and K_B are the impedance terms of the boulder within the embedding soil, and R_B is the boulder ultimate resistance to displacement within the embedding soil.

The mechanical model is developed within the lumped parameter software GRLWEAP (2010) through user-defined elements representing the interacting boulder. It is emphasized that the model within GRLWEAP rests on two major assumptions: (1) material behaviour and interaction laws are linear and (2) only axial behaviour is modelled. The numerical analysis can output the load exerted by the obstructing boulder as a result of the hammer generated incoming wave force $F_d\downarrow$. The peak contact force can be compared to the minimum axial force required to initiate local pile tip buckling, i.e. Equation 1 and Equation 3.

3 SOIL LIMIT STATES

3.1 *Boulder-soil model*

The mechanical impedance terms C_B and K_B of the boulder within the embedding soil medium can be evaluated using shape and geometrical factors depending on the boulder size and using the mass and deformation properties of the matrix soil.

Although a boulder may take various shapes, it can be assumed for the sake of simplicity to have an axisymmetric ellipsoidal shape, characterised by a diameter in the horizontal plane and by a given height. In the present analysis, the boulder diameter and height were defined by a 1.5:1 (H:V) ratio. It is assumed to be impacted at its very top with a view to remain under a 1D axial framework.

It is further assumed that the boulder possesses a much higher modulus than that of the embedding medium thus allowing us to consider, for service limit state assessments, the boulder as a rigid body embedded in an elastic medium.

As a result, the low-strain stiffness and damping coefficients of the solid boulder in the vertical direction about its initial position (K_B against vertical displacement and C_B against vertical velocity, respectively) will depend on the boulder geometry and on the density ρ and shear modulus G of the embedding medium as follows:

$$K_B = \alpha G a \tag{4}$$

$$C_B = \beta \sqrt{\rho G}\, a^2 \tag{5}$$

where a is the radius of the boulder in the horizontal while α and β are shape factors that can be assessed based on Selvadurai (1980) for a disk and on Chadwick & Trowbridge (1967) for a sphere, following an equivalency principle developed by Lysmer (1966). Values of 15 and 7 have been adopted here for α and β, respectively. It should be noted that a Poisson's ratio of 0.5 can be adopted to reflect the undrained behavior of the embedding medium under transient loading conditions.

Following Equations 4 and 5, the impedance of e.g. a 1 m wide and 0.67 m high axisymmetric boulder with a volume of 0.35 m^3 and a weight of approximately 0.94 t, assuming a density ρ_{rock} of 2.7 t/m^3, and embedded within a stiff till (boulder clay) matrix with $G = 60$ MN/m^2, may be characterized by an embedment stiffness K_B of 450 MN/m and a geometrical damping C_B of 0.62 MN/ms^{-1}.

3.2 *Vertical penetration and deviation*

At large vertical displacements, elasticity can no longer be assumed to evaluate the behavior of the boulder. Several soil failure mechanisms within the embedding medium can be speculated to address ultimate limit state conditions, some of which are illustrated on Figure 2. We have assumed the simple case shown in Figure 2a (or Figure 1) to remain within a 1D framework. This can be considered as a drastic assumption since most of the times, it can be expected that the pile will not hit the boulder at the vertex of its resistance center, as shown e.g. in Figure 2b.

The ultimate resistance of the boulder R_B to a vertical displacement can be assessed based on the undrained shear strength S_u of the embedding medium, using a classical formula of the following type:

$$R_B = N_c\, S_u\, \pi a^2 \tag{6}$$

where N_c is a shape factor that can be assessed based on sphere penetration research; e.g. Randolph et al. (2000). A value N_c of 15 has been adopted here.

Thus, once embedded within a soil medium with $S_u = 300$ kN/m^2, as is typical for stiff glacial till, a 1 m wide boulder can be expected to have an ultimate vertical resistance to penetration of approximately $R_B = 3.5$ MN.

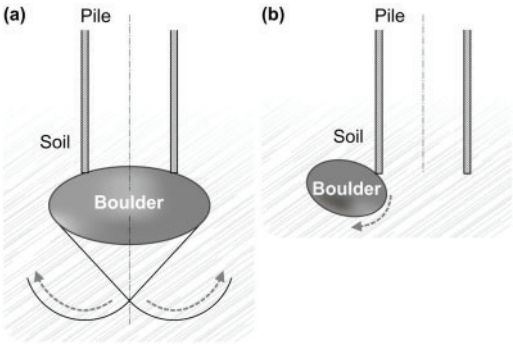

Figure 2. Assumed and potential soil failure mechanisms.

4 BOULDER LIMIT STATES

4.1 *Pile-boulder contact*

The boulder-pile contacting stiffness can be assessed at low strain using elastic solutions pertaining to both bodies: k_s represents the stiffness of the pile contact, evaluated based on the tube wall thickness t and Young modulus of the steel E_{steel}, while k_c represents the stiffness of the boulder contact, evaluated based on the pile wall thickness t, the radius of curvature of the boulder at the contacting point, and the rock deformation modulus. Several approximations of the geometry of the tube toe and boulder in the vicinity of their contact can be made to assess a global contact stiffness based on original developments by Hertz (1882). It should be noted that the load-interpenetration relationships evidenced by Hertz using elasticity theory are not linear, reflecting the progressive growth of the contacting area between the two elastic bodies as the load increases.

4.2 *Modes of boulder failure*

Because of the limited intrinsic strength of the rock forming the boulder, other ultimate limit states have to be considered, involving failure of the boulder itself. Two possible mechanisms are for example illustrated in Figure 3. Figure 3a shows a local failure of the boulder due to the pile wall penetration into it, while Figure 3b illustrates boulder splitting or shearing.

These failure modes require that the strength of the rock be characterised under triaxial loading. To that end, the Hoek-Brown (1997) criterion can be adopted. This criterion calls upon several parameters, including rock mass GSI (Geological Strength Index) describing rock weathering and fissuring, on top of a reference "intact" rock strength.

For our sample problem, we have adopted a rock Unconfined Compressive Strength (UCS) $\sigma_{c,rock}$ of 40 MN/m^2 and a shear strength τ_{rock} of 6 MN/m^2.

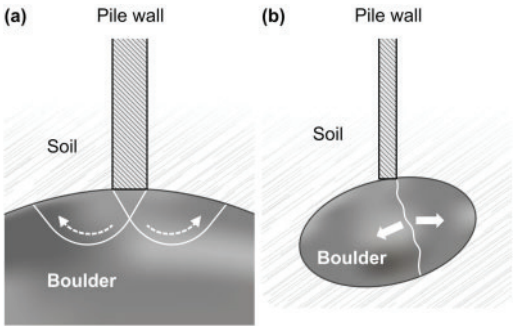

Figure 3. Assumed boulder failure mechanisms.

Table 1. Summary of applied parameters.

Property Description	Value
Pile diameter, D	6 m
Pile wall thickness, t	80 mm
Pile/Steel Young's modulus, E_{steel}	210,000 MN/m^2
Pile/Steel yield stress, σ_y	325 MN/m^2
Hammer type Menck MHU	1500S
Hammer operational energy setting	70%
Boulder geometry (width)	1 m
Boulder geometry (height)	0.67 m
Boulder density, ρ_{rock}	2.7 t/m^3
Boulder/rock Young's modulus, E_{rock}	26,700 MN/m^2
Boulder/rock UCS, $\sigma_{c,rock}$	40 MN/m^2
Boulder/rock shear strength, τ_{rock}	6 MN/m^2
Soil matrix (stiff till) shear strength, S_u	300 kN/m^2
Soil matrix (stiff till) shear modulus, G	60 MN/m^2

These values lead to an estimate of the limit penetration pressure of the steel wall into the boulder that exceeds the yield strength of the steel.

5 SAMPLE ANALYSES

5.1 *Case considered*

The methodology presented in Section 4 has been applied considering the elements listed in Table 1.

The pile mechanical impedance can be ascertained as $I_p = 60.4\,\text{MN/ms}^{-1}$. Application of Equation 3 leads to a pile axial yield force F_{axial} of 5.8 MN to initiate a local dent. The mechanical parameters listed above lead to a pile-boulder tangent contacting stiffness (compliance $= 1/k_s + 1/k_c$) of the order of 1900 MN/m, under that reference load.

A very long pile has been modelled to isolate the pile-boulder interaction from the effects of a 25 MN assumed skin friction. GRLWEAP models the pile itself by a succession of masses and springs and the boulder itself has been modelled by an equivalent pile.

A splice element has been introduced between the pile toe and the boulder to emulate the contact law and disallow tension forces. The tangent stiffness increases with the load until the load reaches the pile reference

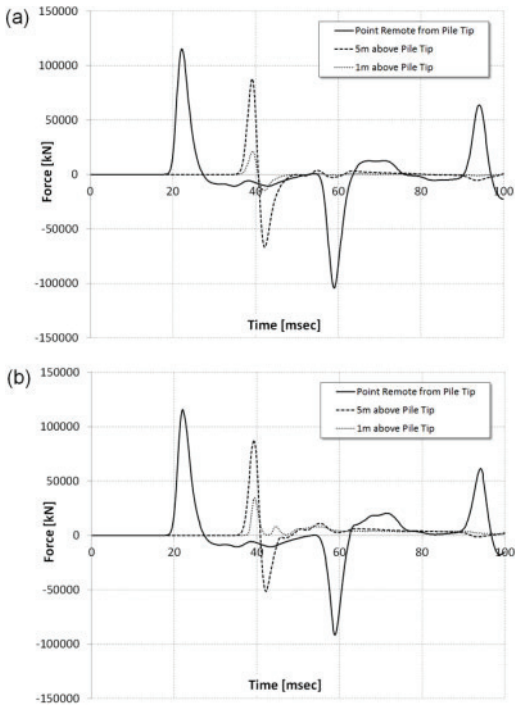

Figure 4. Force signals corresponding to (a) free pile toe and (b) toe in contact with 1 m boulder.

yield load F_{axial} of 5.8 MN. It then remains constant beyond that threshold, which is found compatible with the onset of yielding of the steel within the contact zone.

5.2 *Results*

Figure 4a presents the evaluated force as a function of time at a point remote from the pile tip (solid line for a point located approximately 90 m above the pile toe) and in the vicinity of the pile tip (dotted line) along with the incoming (downward) force $F_d\downarrow$ generated by the hammer for a free-ended pile.

That reference case confirms an amplitude of the incoming compressive force $F_d\downarrow$ in the order of 120 MN. At one meter above the pile tip, it can be noted that the force is not negligible ($\approx$20 MN), as a result of GRLWEAP modeling wave reflections using a lumped parameter approach.

Figure 4b presents the same diagram when the 1 m boulder is added to the pile tip. The force diagram in the vicinity of the pile tip is much higher than that calculated in the first case, but contains interference with clean end modelling conditions. The local load generated by the boulder can be better ascertained by comparing two GRLWEAP analyses at several points.

The difference between pairs of corresponding force signals such as those shown on Figures 4a and 4b can be used with a view to mitigate such artefacts. This approach allowed the authors to estimate that the

peak dynamic force $F_{contact}$ endured by the pile tip at its contact with the boulder is, for the parameters listed above, approximately 11.6 MN. Since this peak contact load is clearly in excess of the pile local yield load F_{axial} (5.8 MN), one must check whether the soil or boulder would not fail before the steel tube would locally yield.

5.3 *Soil and boulder failure*

The peak axial contact load $F_{contact}$ of 11.6 MN obtained by the contact model in the wave equation analysis is actually larger than the boulder ultimate resistance to penetration within the soil matrix ($R_B = 3.5$ MN, see Section 3.2). This indicates that the driving force acting on the boulder is able to plastically displace the boulder within its soil matrix.

If the boulder is centered right beneath the pile wall and the soil reactions are symmetrical, its shear force can be approximated as half the peak contact load. The resulting 5.8 MN shear force (1/2 $F_{contact}$) can be compared to the shear resistance offered by the area defined by a vertical cross-section of the boulder. For the selected rock properties, it is found that that the shear or splitting resistance of the boulder $T_{b,split}$ is at most 3.2 MN, which means that the boulder would be split before it would get vertically displaced.

5.4 *Influence of boulder size*

A parametric analysis of the boulder size can be conducted to explore its influence on the various limit loads considered above. Figure 5 shows the results of such an analysis keeping constant the aspect ratio of the boulder. It should be noted that the boulder shear strength has been estimated based on a scaling law inspired by Heuze (1980) to reflect the higher probability to encounter weaknesses within a larger boulder. While a detailed discussion of scaling laws is beyond the scope of this paper, the experimental data compiled by Heuze suggest a non-linear decrease in rock strength with respect to its intact rock strength as a function of specimen size.

Figure 5 plots the likely increase in boulder penetration resistance R_b (solid line) and boulder splitting resistance $T_{b,split}$ (dotted line) with increasing boulder width and compares these with the pile axial yield limit F_{axial} (dashed line) and calculated peak dynamic contact force $F_{contact}$ for a 1 m and 2.5 m wide boulder, assuming a 70% hammer operational energy setting.

It can be observed from Figure 5 that, for the case considered and within the represented range of boulder size:

- The peak driving force potentially transmitted to the boulder exceeds the pile yield load F_{axial}, the boulder splitting resistance $T_{b,split}$, and to some extent the soil limit load (boulder penetration resistance R_b);
- The mode of failure depends on boulder size.

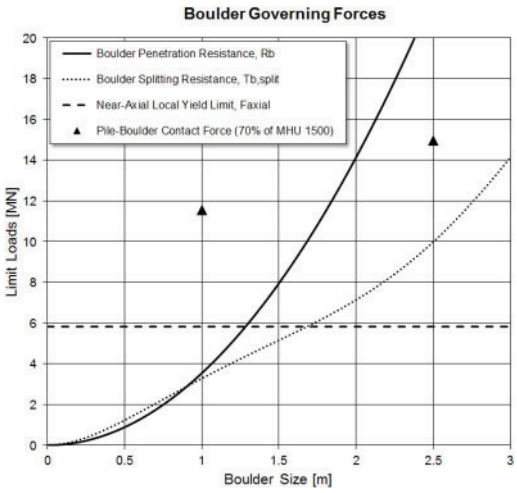

Figure 5. Limit loads of pile, boulder and soil as functions of boulder diameter.

6 CONCLUSIONS

A novel approach has been suggested to assess the pile-boulder encounter within an axial framework. The approach rests on the modelling of (1) the pile, using its 1-D longitudinal wave equation, (2) the boulder, based on its shape, mass, and mechanical impedance properties of its embedding medium, and (3) their contact law, based on elastic theory up to the pile yield load. The application of the proposed methodology to a 1 m wide boulder embedded in stiff glacial till indicates that the local contacting force under a typical hammer blow would clearly exceed the quasi axial yield load of an 80 mm thick walled 6 m diameter pile.

The need to define boulder size and fully characterize boulder strength with respect to breaking/splitting modes is highlighted.

In practice, such analysis may prove useful in estimating the risk of local pile tip yielding or initial dent formation during driving in boulder prone formations, whether the obstructing boulder can be displaced within the soil matrix, and the ensuing risk of pile damage propagation should local pile tip yielding occur. Depending on the risk assessment, counter-measures such as increased pile tip wall thickness combined with lower hammer operational energy settings may be employed to mitigate the risk of pile damage.

REFERENCES

Aldridge, T.R., Carrington, T.M. & Kee, N.R. 2005. Propagation of pile tip damage during installation, in 1st International Symposium on Frontiers in Offshore *Geotechnics*, 19–21 September 2005, Perth, pp. 823–827.

Alm, T., Snell, R.O., Hampson, K.M. & Olaussen, A. 2004. Design and Installation of the Valhall Piggyback Structures, *Offshore Technology Conference* (OTC) 16294, Houston, Texas, 3–6 May 2004.

Barbour, R.J. & Erbrich, C.T. 1995. Analysis if Soil-Skirt Interaction During Installation of Bucket Foundations Using ABAQUS, in *Proceedings ABAQUS Users Conference,* Paris, France, May 1995.

Chadwick, P. & Trowbridge, E.A. 1967. Oscillations of a rigid sphere embedded in an infinite elastic solid, II: rectilinear oscillations, *Proc. Camb. Phil. Soc.*, 63, pp. 1207–1227.

Erbrich, C.T., Barbosa-Cruz, E. & Barbour, R. 2010. Soil-pile interaction during extrusion of an initially deformed pile, in *Frontiers in Offshore Geotechnics II,* CRC Press.

GRLWEAP 2010. Wave equation Analysis of Pile Driving, Version 2010.

Heuze, F.E. 1980. Scale effects in the determination of rock mass strength and deformability, in *Rock Mechanics*, Volume 12, Issue 3–4, March 1980, pp. 167–192.

Hertz, H. 1882. Über die Berührung fester elastischer Körper (On the contact of elastic solids), *Journal fur die Reine und Angewandte Matematik*, Vol. 92, pp. 156–171.

HSE. 2001. A study of pile fatigue driving and in-service and of pile tip integrity, prepared for the *Health and Safety Executive* by MSL Engineering Limited.

Hoek, E. & Brown, E.T. 1997. Practical estimates of rock mass strength, *International Journal of Rock Mechanics and Mining Sciences,* Vol. 34, N° 8, 1997, pp. 1165–1186.

Philip, A.L. 1990. Ice-Pushed Boulders on the Shores of Gotland, Sweden, in *Journal of Coastal Research*, Volume 6, Issue 3, Summer 1990, pp. 661–676.

Randolph, M.F., Martin, C.M. & Hu, Y. 2000. Limiting resistance of a spherical penetrometer in cohesive material, *Geotechnique*, 2000

Selvadurai, A.P.S. 1980. The dynamic response of a rigid circular foundation embedded in an isotropic elastic medium of infinite extent, *Proc. Intl. Symp. Soils under Cyclic and Transient Loadings* (Pande and Zienkiewicz Eds.), Swansea, U.K., Vol. 2, Balkema, The Nertherlands, pp. 597–608.